Catalysts **2015**, *5*, 851-867; doi:10.3390/catal5020851

OPEN ACCESS

catalysts

ISSN 2073-4344

www.mdpi.com/journal/catalysts

Article

Co-Al Mixed Oxides Prepared via LDH Route Using Microwaves or Ultrasound: Application for Catalytic Toluene Total Oxidation

Eric Genty [1], Julien Brunet [1], Christophe Poupin [1], Sandra Casale [2], Sylvie Capelle [1], Pascale Massiani [2], Stéphane Siffert [1,*] and Renaud Cousin [1,*]

[1] Unité de Chimie Environnementale et Interactions sur le Vivant (UCEIV, EA 4492), Université du Littoral Côte d'Opale (ULCO), 145 avenue Maurice Schumann, 59140 Dunkerque, France; E-Mails: Eric.Genty@ulb.ac.be (E.G.); Julien.Brunet@univ-littoral.fr (J.B.); Christophe.Poupin@univ-littoral.fr (C.P.); Sylvie.Capelle@univ-littoral.fr (S.C.)

[2] Laboratoire de Réactivité de Surface (LRS), CNRS UMR 7197, Sorbonne Université, Université Pierre et Marie CURIE (UPMC), 4 place Jussieu, 75005 Paris, France; E-Mails: sandra.casale@upmc.fr (S.C.); pascale.massiani@upmc.fr (P.M.)

* Authors to whom correspondence should be addressed; E-Mails: stéphane.siffert@univ-littoral.fr (S.S.); renaud.cousin@univ-littoral.fr (R.C.); Tel.: +33-03-2865-8256 (S.S.); +33-03-2865-8276 (R.C.); Fax: +33-03-2865-8239 (S.S. & R.C.).

Academic Editor: Jean-François Lamonier

Received: 27 February 2015 / Accepted: 4 May 2015 / Published: 15 May 2015

Abstract: Co_6Al_2HT hydrotalcite-like compounds were synthesized by three different methods: co-precipitation, microwaves-assisted and ultrasound-assisted methods. The mixed oxides obtained after calcination were studied by several techniques: XRD, TEM, H_2-TPR and XPS. They were also tested as catalysts in the reaction of total oxidation of toluene. The physico-chemical studies revealed a modification of the structural characteristics (surface area, morphology) as well as of the reducibility of the formed mixed oxides. The solid prepared by microwaves-assisted synthesis was the most active. Furthermore, a relationship between the ratio of Co^{2+} on the surface, the reducibility of the Co-Al mixed oxide and the T_{50} in toluene oxidation was demonstrated. This suggests a Mars Van Krevelen mechanism for toluene total oxidation on these catalysts.

Keywords: mixed oxide; LDH; microwaves; ultrasound; toluene; catalytic oxidation

1. Introduction

The emissions of Volatile Organic Compounds (VOCs) in industrial activities are now strictly regulated due to their harmfulness towards public health and the atmospheric environment. Among the many technologies available for VOCs control, catalytic oxidation of these pollutants to carbon dioxide and water has been recognized as one of the most promising ones. Supported noble metals are generally considered as efficient catalysts for VOCs oxidation [1–5] and their efficiency at low temperature can sometimes be considered as a key advantage favoring the use of such catalysts compared with mixed oxide catalysts. However, due to the high cost of noble metals, many researchers have recently devoted strong efforts to the development of suitable catalysts containing only transition metal oxides [6–10]. In this domain, special attention has been focused on cobalt materials in the spinel form [10], on oxide catalysts [11,12] and on mixed oxides issued from hydrotalcite precursors [13,14]. For the generation of well-dispersed, active and very stable mixed oxides, the Layered Double Hydroxides (LDH) route shows much potential. Indeed, LDH, also referred to as hydrotalcite-like compounds, constitute a large group of natural and synthetic minerals whose physico-chemical properties have strong analogies with clay minerals and more particularly with cationic clay minerals. This class of layered double hydroxides consists of positively charged metal hydroxide layers separated from each other by anions and water molecules. The wide range of possible cations and anions that can be incorporated in the Hydrotalcite (HT) structure gives rise to a large number of materials [7,13,14]. In addition, a high surface area, a good thermal stability, a good mixed oxides homogeneity, basic properties and a high metal dispersion are obtained after thermal treatment [10,15].

The interest in applying calcined LDH as catalysts in the environmental field has already been demonstrated. For example, mixed oxides have been shown to be very active and selective in the decomposition of nitrogen oxides [16] or in the total oxidation of Volatile Organic Compounds [13,14]. Also, mixed oxides obtained after calcination were used equally as catalysts [13,17] or as catalytic support [18–20] in redox reactions such as the selective oxidation of hydrocarbons or the total oxidation of VOCs [21,22].

The conventional and most widely used method to prepare LDH is co-precipitation [7,8,13,14]. However, alternative methods providing well-crystallized materials have also been studied [23,24]. In particular, the use of microwaves during the synthesis of catalytic materials presented several advantages over conventional methods. Thus, Ran *et al.* [24] have synthesized ternary oxides of $La_{0.7}Sr_{0.3}MnO_{3+\lambda}$ using microwaves and they have highlighted the benefits of this synthesis method, compared to conventional sol-gel synthesis, in terms of rapidity (3–5 min compared to several hours), energy efficiency, uniformity of heating (no hot spot in the solution), homogeneity of the obtained solid (larger specific surface area and small particle sizes). Kaddouri *et al.* [25] showed that a $La_{1-x}B_xMnO_{3.15}$ perovskite type solid synthesized under microwaves exhibit better catalytic properties than the same solid synthesized conventionally. Similarly, the use of ultrasounds in the synthesis of material was reported to be beneficial due to the phenomenon of acoustic cavitation that corresponds to the formation, growth and collapse of bubbles generated in the solution. Zhou *et al.* [26] performed the impregnation of zirconium and cobalt supported on SiO_2 ($Co/Zr/SiO_2$) with sonication and they noted that ultrasounds increase the specific surface area and lead to a better dispersion of the cobalt particles on the substrate surface due to such cavitation effects. Similar cavitation phenomena have allowed obtaining a better

catalytic reactivity of solids in the Fischer-Tropsch reaction. Recently, microwaves radiation heating [27–29] and ultrasound [27,30,31] have been applied to the synthesis of hydrotalcites with different chemical compositions as an alternative to the conventional hydrothermal treatments. Several of the advantages listed above have been observed, especially the shorter treatment times needed to achieve enhanced crystallinity degrees, the higher specific surface area and the improved metallic dispersions [28,32,33].

A previous study in our laboratory has shown that Co-Al mixed oxide catalysts present interesting catalytic activity for total oxidation of toluene [13]. In order to improve this type of catalytic materials, the aim of the present work was to investigate the effect of treatment by microwaves or by ultrasound during the preparation of the LDH samples. Thus, mixed oxides were prepared by calcination of hydrotalcite like compounds precursors (Co_6Al_2HT and Mg_6Al_2HT) using three different routes (microwaves (MW), ultrasound (US) and conventional treatment (CT)) and the catalytic properties of the samples were tested in the total oxidation of toluene. The mixed oxide properties were also characterized by several techniques: powder X-ray Diffraction (XRD), Transmission Electron Microscopy (TEM) Hydrogen Temperature Programmed Reduction (H_2-TPR) and X-ray photoelectron spectrometry (XPS).

2. Results and Discussion

Table 1 indicates the code names and the specific surface areas of the mixed oxides obtained after calcination of the hydrotalcite precursors. With the aim to study the effect of the preparation method, the cobalt-based materials are compared in this table to reference Mg-Al-O materials having more conventional hydrotalcite compositions but synthesized following the same protocols as those used for the preparation of the Co-Al mixed oxides. Compared to the samples prepared by coprecipitation, a significant increase of the specific surface area is observed when the mixed oxides were prepared using either the US or the MW method. This result was already reported in the literature [28,30,31]. Indeed, Neto *et al.* [31] have shown on LDH synthesis by sonication that ultrasounds not only accelerate crystal formation but also better disperse small particles, thus reducing their aggregation during nucleation and crystal growth and giving rise to increased specific surface area. Moreover, concerning the effect of microwaves during the LDH preparation, it was observed that MW radiation for short time leads to faster nucleation, which produces a larger number of small crystals and therefore an increase of the surface area [28]. Thus, the treatment by microwaves or by ultrasounds during synthesis improves the specific area of the obtained materials.

Table 1 also reports the chemical compositions of the solids. It can be clearly seen that the ratio $M^{2+}/Al^{3+} = 3$ is well respected for each solid. The T_{50} values reported as well in Table 1 (temperature at which 50% of the toluene is converted) show that the catalytic performances of the samples in toluene total oxidation follow the order:

$$Co_6Al_2HTMW500 > Co_6Al_2HTUS500 > Co_6Al_2HTCT500 >> Mg_6Al_2HTMW500 > Mg_6Al_2HTUS500 > Mg_6Al_2HTCT500 \quad (1)$$

This order is also illustrated in Figure 1 that shows the evolution of the conversion levels as a function of the temperature. From these data, it can be concluded that the replacement of the bivalent cation Mg^{2+}

by Co^{2+} in the chemical composition of sample has a significant effect. This observation is in line with a previous work [13] that indicated the importance of the nature of the bivalent cation in the sample. Moreover, an increase of the catalytic activity is clearly observed for the solids prepared by microwaves or ultrasounds methods.

Table 1. Code name, BET specific area, chemical composition, crystallite size and temperature of 50% toluene conversion (T_{50}) of catalysts.

Solids	Specific surface area ($m^2 \cdot g^{-1}$)	Chemical composition M^{2+}/Al^{3+}		T_{50} (°C)	Crystallite size of oxide * (nm)
		Theoretical	Experimental		
Mg_6Al_2HTCT500	216	3	2.79	477	11.6
Mg_6Al_2HTUS500	272	3	2.84	421	4.5
Mg_6Al_2HTMW500	342	3	2.95	395	3.7
Co_6Al_2HTCT500	123	3	2.85	287	9.4
Co_6Al_2HTUS500	157	3	3.15	278	7.0
Co_6Al_2HTMW500	167	3	3.00	271	7.6

* Estimated by the XRD measurement.

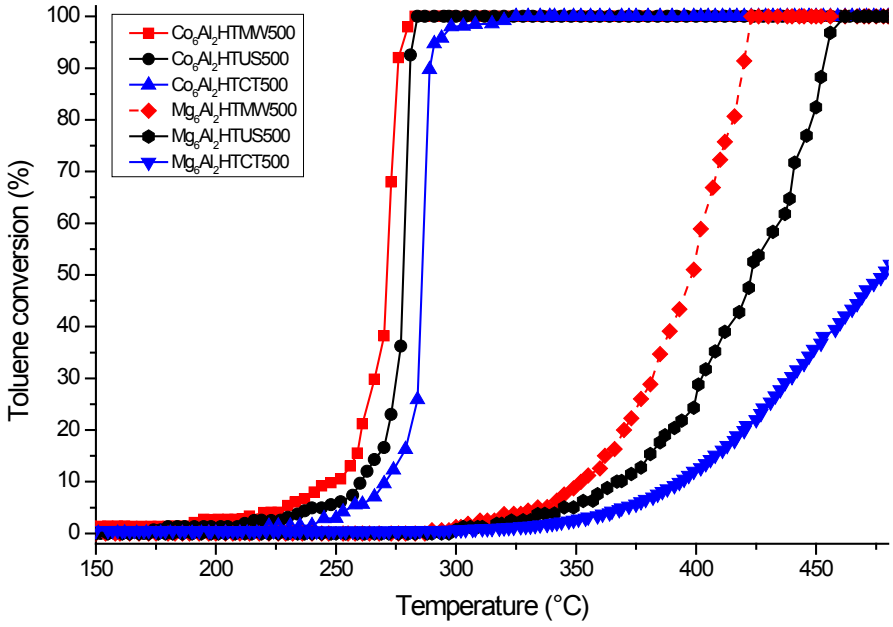

Figure 1. Conversion of toluene (%) on mixed oxide *vs.* reaction temperature (°C).

When toluene conversion was complete, H_2O and CO_2 were the only products observed. However, during toluene conversion at lower temperatures on fall samples, few ppm of benzene and CO were detected. Different reaction paths have been already recognized [34]. The most important reaction route is the one initiated by attack on the methyl group with subsequent oxidation steps; however, direct dealkylation of toluene into benzene is possible.

For a better understanding of the effect of these preparation methods on the catalysts, physico-chemicals characterizations of the Co-Al mixed oxides were performed. Firstly, XRD was done to investigate the structure of the samples. The X-ray diffraction patterns (Figure 2) reveal several crystalline spinel phases. These spinel phases are divided into two groups: the spinel phase of cobalt (II)

and cobalt (III) (Co_3O_4 (JCPDS-ICDD 42-1467)) and cobalt aluminum spinel $CoAl_2O_4$ phases (JCPDS-ICDD 44-0160) and Co_2AlO_4 (JCPDS-ICDD 38-0814). The presence of the first phase (Co_3O_4) is due to the easy oxidation of Co^{2+} to Co^{3+} in contact with the air and the greater thermodynamic stability of this phase compared to CoO [35]. However, the three diffraction patterns of these three spinel phases are very similar in position and in intensity [36–38]. For this reason, it is not possible to differentiate the phases by XRD. The Co-Al mixed oxide leads to the normal spinel, *i.e.*, $CoAl_2O_4$ corresponding to the Co^{2+} in the tetrahedral positions and the Al^{3+} in the octahedral position. However, a slight decrease in the crystallite size of the oxide is observed for solids prepared using the microwaves or ultrasound methods (Table 1).

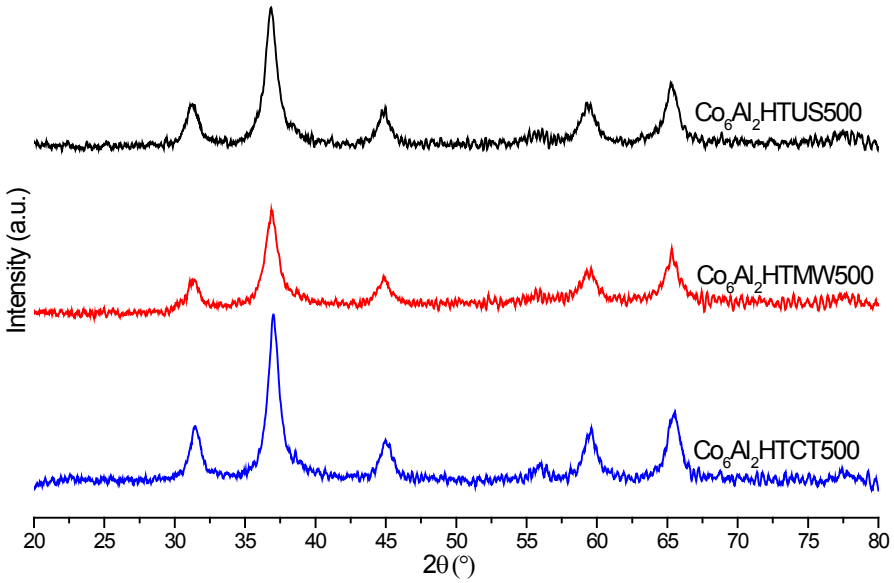

Figure 2. X-ray diffraction patterns of the mixed oxides.

In order to investigate the morphology of the samples prepared via the three different routes, TEM analysis was performed. From the representative micrographs shown in Figure 3, some morphological differences can be observed depending on the cobalt based mixed oxide. Firstly, the SEM images show that the three samples are formed of agglomerates (with sizes in the mm range), themselves composed of an aggregation of very small particles. As seen by both SEM (Figure 3a–c) and TEM (Figure 3a′–c′) images, the size of these individual particles is bigger and less regular in the solid resulting from the conventional synthesis. By contrast, the other two samples have a sharper size distribution of grains with more uniform particle sizes, less than 10 nm. Moreover, the grains appear much thinner, especially in the case of Co_6Al_2HTMW500 (see insets in SEM images). These observations are consistent with the assessment of the crystallite size made during the XRD analysis (Table 1). Moreover, the HR-TEM images confirm that all three samples are composed of grains with crystalline structure. Finally, the various TEM images suggest a difference in porosity among the three samples, being more important on the solid resulting from both the Ultrasonic and microwave assisted syntheses compared to the solid issued from the conventional route.

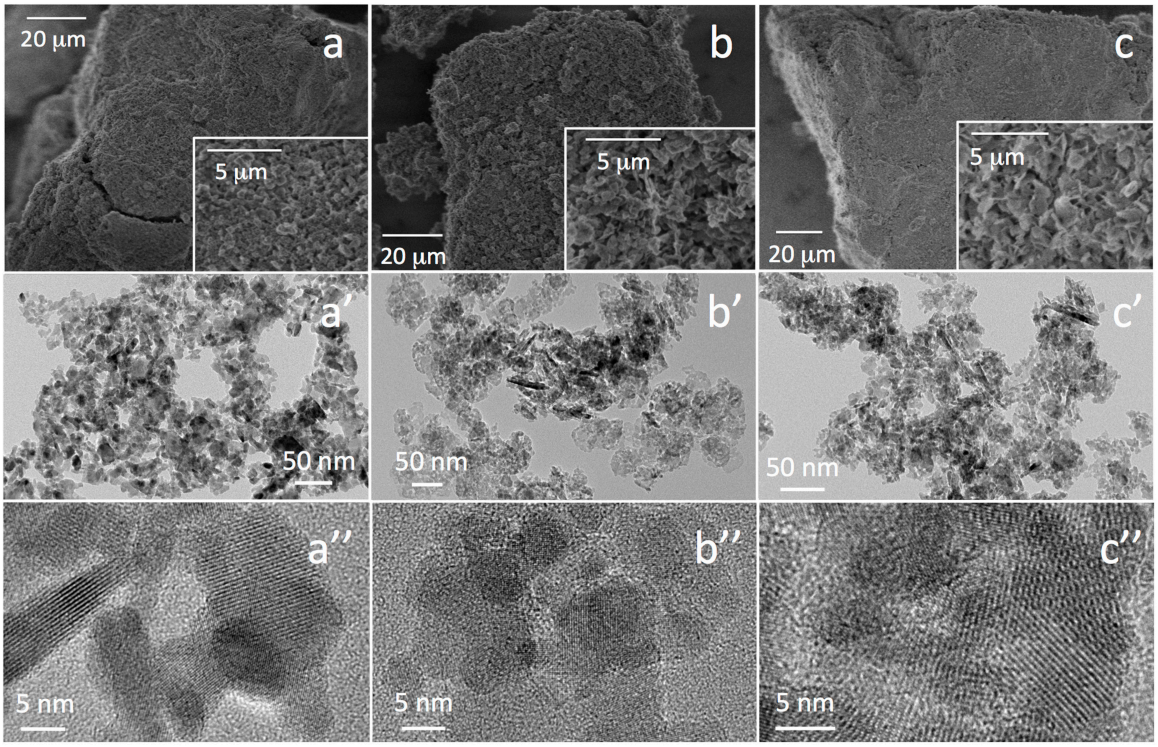

Figure 3. (**a**–**c**) SEM; (**a′**–**c′**) TEM and (**a″**–**c″**) HR-TEM images of samples of (**a**,**a′**,**a″**) Co_6Al_2HTCT500, (**b**,**b′**,**b″**) Co_6Al_2HTUS500 and (**c**,**c′**,**c″**) Co_6Al_2HTMW500.

Regarding the grains morphology, each grain has solid elliptical shapes of larger or smaller size. However, in the case of solids issued from unconventional syntheses, the presence of elongated grains forms ("rods") is observed. This form of grain may be due to two factors: the orientation of the grain in the analysis is perpendicular to the plane or the grain has "rod" type morphology. Such rod shape morphology has been already observed in the literature for solid cobalt oxide (Co_3O_4) [39,40] and it has been interestingly related to samples having good performances in the oxidation of carbon monoxide at low temperatures.

Analysis of the samples by Temperature-Programmed Reduction (H_2-TPR) was next performed (Figure 4). The reduction profile has a similar shape for the three samples but the reduction temperature of samples slightly differs depending on the preparation method of the solid. Indeed, the solid resulting from the synthesis with microwaves is reduced at lower temperatures. In order to identify more specifically the reduction peaks, deconvolution of these peaks using Gaussian-type components was done. This peak deconvolution (Figure 4), with a correlation factor greater than 0.999, reveal that the reduction of Co_6Al_2HT500 consists of two steps at low temperatures ($T < 400$ °C) for the Co_3O_4 species and three steps at high temperature ($T > 400$ °C) for cobalt/aluminum spinel species [39,41–43].

At $T < 400$ °C

$$Co_3O_4 + H_2 \rightarrow 3CoO + H_2O \quad (2)$$

$$3CoO + 3H_2 \rightarrow 3Co + 3H_2O \quad (3)$$

At $T > 400$ °C

$$2Co_2AlO_4 + H_2 \rightarrow CoAl_2O_4 + 3CoO + H_2O \quad (4)$$

$$CoAl_2O_4 + 3CoO + 4H_2 \rightarrow 4Co + Al_2O_3 + 4H_2O \quad (5)$$

$$CoAl_2O_4 + H_2 \rightarrow Co + Al_2O_3 + H_2O \quad (6)$$

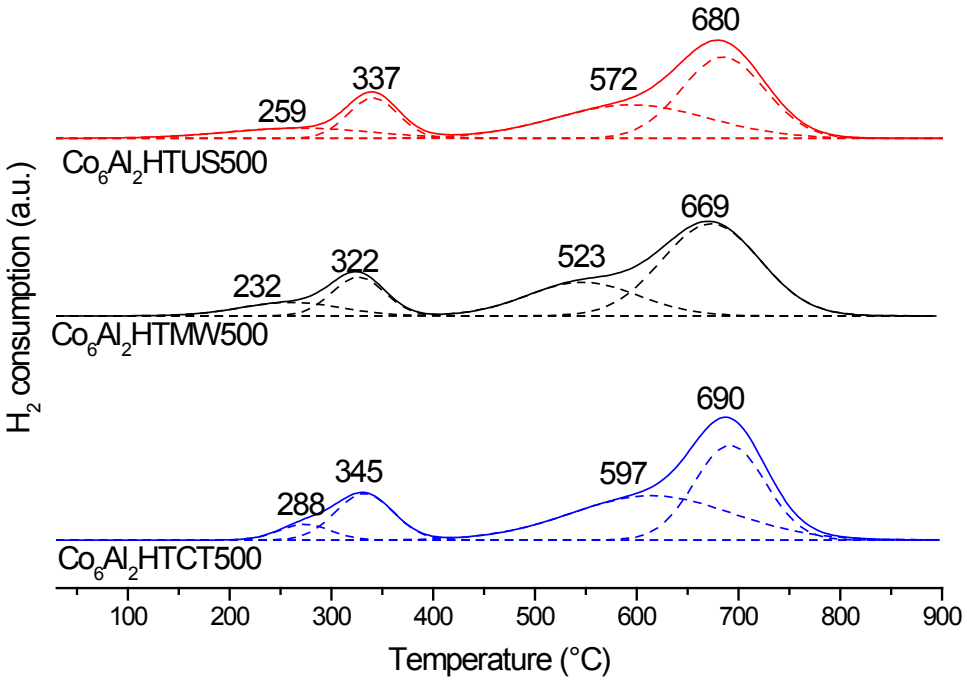

Figure 4. H_2-TPR profiles of the mixed oxides.

For the three solids, a distinction between the two reduction stages of Co_3O_4 is possible. Similar discrimination was done earlier by Moulijn and Arnoldy [41] and explained by the reduction of Co_3O_4 into CoO phase at around 240 °C. Then, the second peak (at 330 °C) corresponds to the reduction of either the CoO phase into Co^0 or of Co_3O_4 into Co^0 [39,41–43]. Regarding the reduction of species at higher temperatures (T > 400 °C), only a limited change in the shape of the profiles is observed. The observation of three stages of reduction is more difficult because they are in the same temperature range. Indeed, a smaller reduction temperature is observed in the case of the solids synthesized using microwaves or ultrasound. Cook *et al.* [44] showed the importance of the crystallite size for the reduction step. Thus, when the crystallite size decreases, the reducibility takes place at lower temperature. The consumption for all peaks is reported into Table 2. The stoichiometry of the first steps (T < 400 °C) predicts a ratio equal to 3 for the consumption ratio peak 2/1. This ratio is respected for all samples, which confirms the hypothesis for the chemical equation. Concerning the second step, it is difficult to distinguish the three steps due to the position in the same temperature range. So, for the quantitative study, the first step ($Co_2AlO_4 \rightarrow CoAl_2O_4$ and CoO) corresponds to Peak 3 and the last two correspond to Peak 4. The ratio between Peaks 4 and 3 is equal to 5 which is in accordance with the literature [39,41–44].

Table 2. Temperatures for H_2 consumptions by TPR experiments Co_6Al_2HT500 issued from different preparation methods.

Catalyst	Temperature (°C) H_2 consumption ($\mu mol \cdot g^{-1}$)				Consumption ratio peak 2/1	Consumption ratio peak 4/3	H_2 consumption ($\mu mol \cdot g^{-1}$)
	Peak 1	Peak 2	Peak 3	Peak 4			
$Co_6Al_2HTCT500$	288 °C 644	345 °C 2012	597 °C 1458	690 °C 7410	3.12	5.08	11715
$Co_6Al_2HTUS500$	259 °C 651	337 °C 2192	572 °C 1557	680 °C 7444	3.36	4.78	11845
$Co_6Al_2HTMW500$	232 °C 777	322 °C 2242	523 °C 1229	669 °C 7711	2.88	4.69	11961

The cobalt based catalysts were also characterized by XPS in order to examine the effect of the preparation method on the nature and the oxidation degrees of the surface species. The XPS spectra of O 1s and Co 2p are shown in Figure 5, and the XPS data are summarized in Table 3.

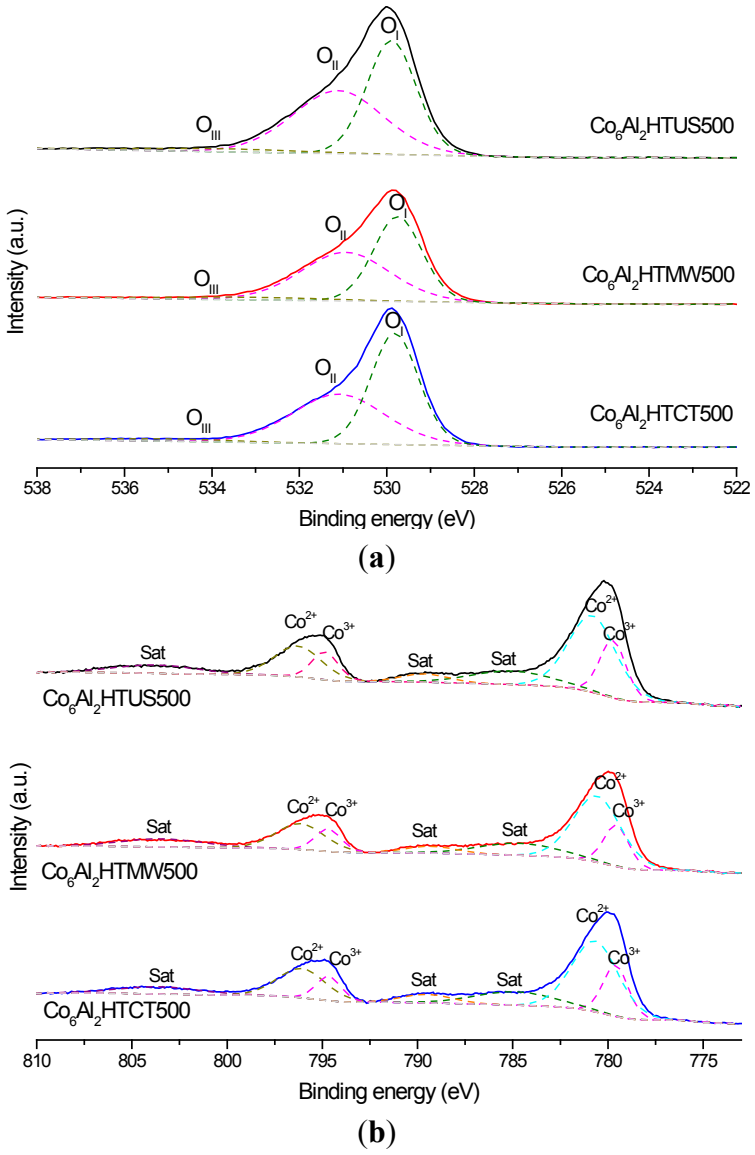

Figure 5. XPS spectra of (**a**) O 1s and (**b**) Co 2p from the mixed oxides.

Table 3. Binding energy (E_b) for O_{1s} and Co_{2p} levels for the catalysts.

Catalyst	E_b (O_{1s}) (eV)			E_b (Co_{2p}) (eV)			
	O_I	O_{II}	O_{III}	Co $2p_{1/2}$		Co $2p_{3/2}$	
				Co^{2+}	Co^{3+}	Co^{2+}	Co^{3+}
Co_6Al_2HTCT500	529.8	531.1	533.9	796.1	794.7	780.7	779.6
Co_6Al_2HTUS500	529.9	531.1	533.8	796.1	794.7	780.8	779.7
Co_6Al_2HTMW500	529.8	531.0	533.5	796.2	794.8	780.7	779.6

Regarding the photopeak of oxygen 1s (O 1s), three components are observed. The first component (O_{III}) at 533–534 eV corresponds to the oxygen present in the form of carbonates or of water molecules [45]. The second component (O_{II}) at 531 eV corresponds to adsorbed surface oxygen (O_2^- or O^-) or hydroxyl groups (HO^-) [46,47]. The last component (O_I) which is located at a lower binding energy is consistent with lattice oxygen O^{2-}. The oxygen composition of the surface of the solid plays an important role in the catalytic activity in the oxidation reactions. Indeed, O_{II} species exhibit greater mobility than the lattice oxygen. In addition, several authors [46,47] have shown that the catalytic activity of the solid could be related to the presence of a relationship between oxygen O_{II} and the largest O_I oxygen. From the data, a ratio between the O_I and O_{II} species was calculated for all samples (Table 4). This revealed that for solids synthetized under ultrasound or microwaves, the ratio O_{II}/O_I increased.

Table 4. XPS data of Co_6Al_2HT500 issued from different preparation methods and catalytic intrinsic activity calculated at 10% toluene conversion.

Catalyst	Surface Content (%) by XPS			T_{50} (°C)	Catalytic intrinsic activity ($mol \cdot m^{-2} \cdot h^{-1}$)
	O_{II}/O_I	Co^{2+}/Co^{3+}	Co/Al		
Co_6Al_2HTCT500	0.86	2.38	2.9	287	2.59×10^{-10}
Co_6Al_2HTUS500	1.01	2.69	2.9	278	2.80×10^{-10}
Co_6Al_2HTMW500	1.05	2.98	3.3	271	3.05×10^{-10}

Concerning the cobalt species (Table 3), an overlay of the photopeaks attributed to Co 2p is represented in Figure 5b. The observed profiles are characteristic of a mixture of Co^{2+} and Co^{3+} belonging to $CoAl_2O_4$ or Co_3O_4 species [48,49]. A relationship between the Co^{2+} and Co^{3+} species was calculated as the ratio of the area of the Co^{2+} signal component Co $2p_{3/2}$ and the Co^{3+} signal component Co $2p_{3/2}$ [6] (Table 4). This ratio suggests that the surface amount of Co^{2+} is higher in the Co_6Al_2HTMW500 solid. It can be observed as well that the presence of oxygen defects is at a higher quantity in the case of the Co_6Al_2HTMW500 mixed oxide, which could explain the best catalytic reactivity of the solid [6,48].

For the VOC oxidation on metal oxide based catalysts, several catalyst parameters, such as the surface area, the reducibility of the active species, the oxidation degree of the metal species or the oxygen species present on the surface, can affect the catalytic performances [6,50]. Thus, the better activity of the mixed oxides synthesized using microwaves can be related to a larger specific surface area. Indeed, this increased surface area can provide greater availability of the active phase for the reaction.

Moreover, a relationship between the H_2 consumption of the first temperature peak (corresponding to the reduction of the phase Co_3O_4 into Co^0) between 0 and 400 °C and the catalytic intrinsic activity is

obtained (Figure 6). This relationship between the low-temperature reducibility and the toluene conversion suggests that Co_3O_4 is the active phase. Then, a redox mechanism for this reaction can be proposed, corresponding to a Mars Van Krevelen mechanism [6,51]. This mechanism involves the participation of the lattice oxygen by a redox cycle. For the combustion of alkane with cobalt oxide, Solsona *et al.* [51] reported that O^{2-} anions participate in the total oxidation according to the redox mechanism. Moreover, Bahlawaue [52] showed that the reactivity depends on the fast migration of oxygen ions through the lattice cobalt oxide.

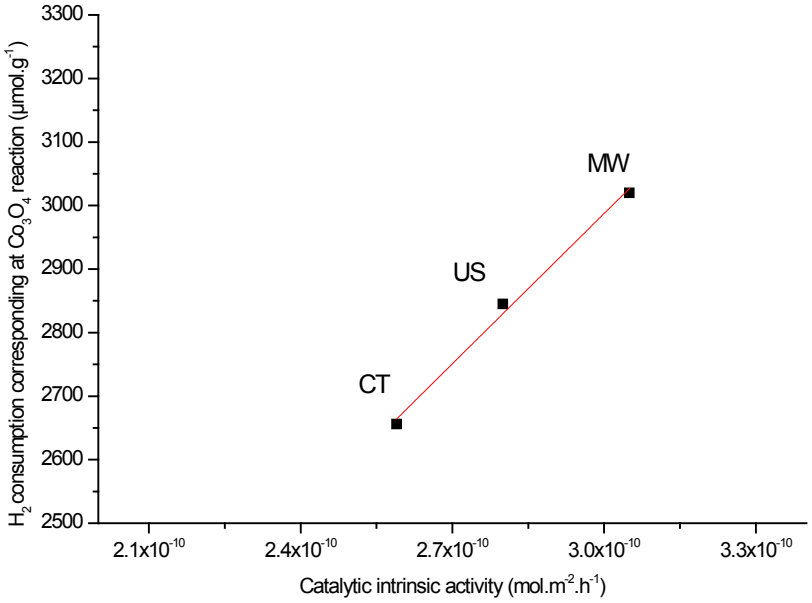

Figure 6. Relationship between catalytic intrinsic activity and H_2 consumption during the H_2-TPR corresponding at Co_3O_4 species.

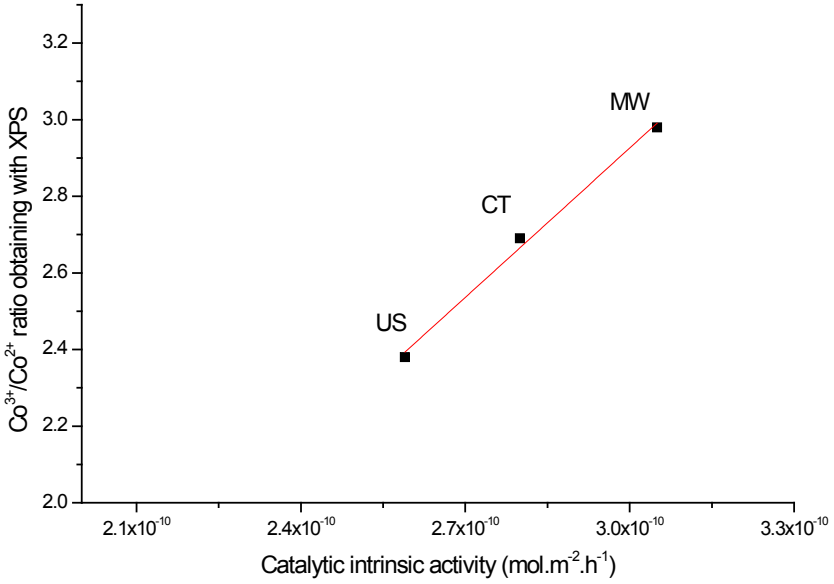

Figure 7. Relationship between catalytic intrinsic activity and the ratio Co^{2+} and Co^{3+} species calculated with XPS analysis.

Moreover, another relationship could be identified as well, involving XPS results. Indeed, Figure 7 shows that the Co^{2+}/Co^{3+} ratio evaluated by XPS is also linearly related to the catalytic intrinsic activity. The relationship shows that the proportion of solid in the Co^{2+} is an important factor for achieving a good activity of the solid. Indeed, Figure 7 shows that the most active solid in the oxidation of toluene has the highest Co^{2+} proportion on the surface of the solid. This can also be linked to the increased presence of O_{II} species (adsorbed oxygen O_2^- or O^- type and oxygen vacancies in the surface of the solid). The greater presence of such a type of oxygen in the case of solids prepared by microwaves and ultrasound is an important feature that provides a higher availability of oxygen to effect the reaction (and the reduction of the solid) at low temperatures. Indeed, this oxygen is more mobile and therefore more available for reaction than in the case of the solid prepared conventionally.

3. Experimental Section

3.1. Preparation of Catalysts

Conventional Hydrotalcite (HT) with Co:Al molar ratio 6:2 was prepared by the coprecipitation method. An aqueous solution containing appropriate amounts of $Co(NO_3)_2$, $6H_2O$ and $Al(NO_3)_3$, $9H_2O$ ions (solution A) was added drop-wise under stirring into an aqueous solution containing Na_2CO_3 and NaOH (solution B). During the synthesis, the temperature and the pH were maintained at 60 °C and 10.5, respectively. The solution was aged at 60 °C during 18 h. Then, the precipitate was filtered, washed several times with hot deionized water (50 °C) and dried at 60 °C for 64 h. The obtained sample was called Co_6Al_2HTCT (where HTCT corresponds to the HT synthetized using the conventional method).

Two other samples were prepared using non-conventional methods involving either microwaves (MW) or ultrasounds (US). The first one was prepared by adding solution A (containing Co^{2+} and Al^{3+} ions, see above) into solution B (containing Na_2CO_3 and NaOH). The obtained gel was aged at 80 °C for 1 h, in a monomode reactor Synthewave Prolabo (Fontenay sous bois, France) 402 (300 W) equipped with an infrared pyrometer control and mechanical stirring. After the precipitate was filtered and washed until pH 7, the solid was dried at 60 °C for 12 h. The sample was labeled Co_6Al_2HTMW (where HTMW corresponds to the hydrotalcite preparation route with the microwaves procedure). The preparation of the last sample was carried out as described above, but adding the aqueous solution (A) containing the metal cations (Co^{2+} and Al^{3+}) onto solution (B) containing the base while simultaneously submitting the mixture to ultrasounds irradiation (Branson sonifier (Danbury, CT, USA) 450 (20 kHz)). This procedure was carried out at atmospheric pressure and at ambient temperature. The precipitate was filtered, washed to eliminate the alkali metals and the nitrate ions until the pH 7, and then dried at 60 °C for 12 h. The sample was labelled Co_6Al_2HTUS (where HTUS corresponds to the HT synthetized using the ultrasound method).

Thermal treatment of all three samples was performed under flow of air (4 $L \cdot h^{-1}$, 1 $°C \cdot min^{-1}$, 4 h at 500 °C). The calcined samples were named Co_6Al_2HTCT500, Co_6Al_2HTMW500 and Co_6Al_2HTUS500.

Reference Mg-Al-O materials were also prepared to allow comparisons. These reference solids, derived from classic hydrotalcite compositions, were synthesized and calcined following the same protocols as the ones presented above for the preparation of Co-Al mixed oxides. These samples were respectively denominated Mg_6Al_2HTCT500, Mg_6Al_2HTMW500 and Mg_6Al_2HTUS500.

3.2. Characterization Techniques

Specific surface areas were evaluated by the BET method using a QSurf M1 apparatus (Thermo Electron, Waltham, MA, USA). The gas adsorbed at −196 °C was pure nitrogen.

Crystalline structures were determined at room temperature from X-ray Diffractograms (XRD) recorded on a D8 Advance from Bruker AXS (Champs-Sur–Marne, France) diffractometer equipped with a copper anode (λ = 1.5406 Å) and a LynxEye Detector. The scattering intensities were measured over an angular range of $10° \leq 2\theta \leq 80°$ for all samples with a step-size of $\Delta(2\theta) = 0.02°$ and a count time of 4 s per step. The diffraction patterns were indexed by comparison with the "Joint Committee on Powder Diffraction Standards" (JCPDS) files. Crystallite sizes were determined (Scherrer equation) using a graphic based profile analysis program (TOPAS from Bruker AXS).

Elemental compositions of samples were analyzed using Inductively Coupled Plasma-Optical Emission Spectrometer (ICP OES, Thermo Electron (Waltham, MA, USA) ICAP 6300 DUO).

Samples morphologies were investigated by Transmission Electron Microscopy observations carried out in scanning (SEM) and transmission (TEM) modes. The SEM images were recorded on a Hitachi (Tokyo, Japan) SU-70 SEM-FEG microscope whereas both TEM and HR-TEM (high resolution) images were obtained on a JEOL (Akishima, Japan) JEM-2010 operating at 200 kV).

X-ray photoelectron spectroscopy (XPS) analyses were conducted on a Kratos (Manchester, UK) Axis Ultra DLD spectrometer with a monochromatic Al Kα (hν = 1486.6 eV) radiation source operated at 15 kV and 15 mA. The binding energy (BE) was calibrated based on the line position of C 1s (285 eV). The CasaXPS processing software (Casa Software Ltd. Teignmouth, UK) was used to estimate the relative abundance of the different species. The surface atomic ratios were calculated by correcting the intensity with theoretical sensibility factors based on the Scofield cross section and using a nonlinear Shirley background.

The atomic composition, N_A/N_B, between A and B was derived from the equation:

$$\frac{N_A}{N_B} = \frac{I_A\,\sigma_A}{I_B\,\sigma_B}\left(\frac{E_{CA}}{E_{CB}}\right)^{-0.23} \quad (7)$$

where σ is the cross section, E_C kinetic energy and I is the intensity of the peak.

Temperature-Programmed Reduction (H_2-TPR) experiments were carried out in an Altamira AMI-200 apparatus (Labor und Analysen Technik GmbH, Garbsen, Germany). Prior to the experiment, the sample (30 mg) was activated under argon at 150 °C for 1 h. The sample was then heated from ambient temperature to 850 °C under H_2 flow (5 vol% in argon 30 mL·min^{-1}) with a heating rate of 5 °C·min^{-1}.

3.3. Catalytic Tests

The activity for toluene total oxidation of the catalysts (100 mg) was measured in a continuous flow system in a fixed bed reactor at atmospheric pressure. Before each test, the catalyst was reactivated *in situ* in flowing air (2 L·h^{-1}) at 500 °C for 4 h. The flow of reactant gases (100 mL·min^{-1} with 1000 ppm of C_7H_8 and 20% O_2 in He) was adjusted using a instrument apparatus constituted of a saturator and mass flow controllers. After reaching a stable flow, the reactants were passed through the catalyst bed and the temperature was increased from room temperature to 500 °C (1 °C·min^{-1}). The feed

and the reactor outflow gases were analyzed on line by a 490 Micro gas chromatography from Agilent Technologies France (les Ulis, France). Model 4400IR infrared analyzers from ADEV srl (Cesano Maderno, Italy) were also used to perform the analysis of both CO and CO_2. The catalysts performance was assessed in terms of T_{50} temperature, defined as the temperature at which 50% conversion was obtained.

Catalytic intrinsic activities were evaluated at 10% of toluene conversion and considering a plug-flow reactor:

$$A = \frac{Q \times 273.15 \times [C_7H_8]_0 \times X}{V_M \times T_{10} \times 10^6 \times m \times S_{BET}} \quad (8)$$

where:

A is the catalytic intrinsic activity ($mol \cdot m^{-2} \cdot h^{-1}$);
Q is the volume flow ($L \cdot h^{-1}$);
V_M is the molar volume ($L \cdot mol^{-1}$);
T_{10} is the catalyst temperature for 10% toluene conversion (K);
$[C_7H_8]_0$ is the toluene initial concentration (ppm);
X is the toluene conversion (%);
m is the catalyst mass (g);
S_{BET} is the specific surface area of the catalyst ($m^2 \cdot g^{-1}$).

4. Conclusions

Co_6Al_2HT hydrotalcite-like compounds were synthesized by three different methods: conventional co-precipitation, methods assisted by microwaves or ultrasounds. The mixed oxides obtained after calcination were studied. The specific surface areas of solids prepared under sonication method or using microwaves radiations are much higher than that obtained by coprecipitation. The H_2-TPR analysis shows a reduction at lower temperatures of the Co_3O_4 species. The XPS study shows that the solid resulting from the synthesis by microwaves leads to a higher content in Co^{2+} species on the sample. These Co^{2+} species induce a higher presence of oxygen vacancies that could explain the higher activity of the catalyst. Moreover, correlations between the T50 of the toluene oxidation and the Co^{2+}/Co^{3+} ratio as well as the H_2 consumption of the solids are evidenced, suggesting a Mars Van-Krevelen mechanism. Thus, the preparation of cobalt-based mixed oxide via a Layer Double Hydroxide synthesis route using treatment by microwaves seems to be efficient to obtain a performing catalyst for VOCs oxidation.

Acknowledgments

The authors thank the Industrial Environmental Research Institute (IRENI) and the European Community (Interreg IV France-Wallonie-Flandres project, REDUGAZ) for financial support. The authors would like to thank Francine Cazier, François Delattre and Pierre-Edouard Danjou for their precious advices about the microwaves and ultrasound synthesis.

Author Contributions

Eric Genty and Julien Brunet performed the synthesis of catalysts, carried out the TPR measurements, contributed to the XPS characterization and catalytic tests. Christophe Poupin achieved the XRD experiments. Sandra Casale and Pascale Massiani realized the TEM analysis. All the authors contributed equally to the data interpretation and discussion. Renaud Cousin and Stéphane Siffert coordinate the manuscript. Eric Genty and Renaud Cousin write the manuscript. Sylvie Capelle and Pascale Massiani improved the manuscript.

Conflicts of Interest

The authors declare no conflict of interest.

References

1. Santos, V.P.; Carabineiro, S.A.C.; Tavares, P.B.; Pereira, M.F.R.; Órfão, J.J.M.; Figueiredo, J.L. Applied Catalysis B: Environmental Oxidation of CO, ethanol and toluene over TiO_2 supported noble metal catalysts. *Appl. Catal. B* **2010**, *99*, 198–205.
2. Liotta, L.F. Catalytic oxidation of volatile organic compounds on supported noble metals. *Appl. Catal. B* **2010**, *100*, 403–412.
3. Barakat, T.; Rooke, J.C.; Genty, E.; Cousin, R.; Siffert, S.; Su, B.-L. Gold catalysts in environmental remediation and water-gas shift technologies. *Energy Environ. Sci.* **2013**, *6*, 371–391.
4. Ordóñez, S.; Bello, L.; Sastre, H.; Rosal, R.; Fernando, V.D. Kinetics of the deep oxidation of benzene , toluene, *n*-hexane and their binary mixtures over a platinum on γ-alumina catalyst. *Appl. Catal. B* **2002**, *38*, 139–149.
5. Scirè, S.; Liotta, L.F. Supported gold catalysts for the total oxidation of volatile organic compounds. *Appl. Catal. B* **2012**, *125*, 222–246.
6. Gao, W.; Zhao, Y.; Liu, J.; Huang, Q.; He, S.; Li, C.; Zhao, J.; Wei, M. Catalytic conversion of syngas to mixed alcohols over CuFe-based catalysts derived from layered double hydroxides. *Catal. Sci. Technol.* **2013**, *3*, 1324–1332.
7. Jiratova, K.; Cuba, P.; Kovanda, F.; Hilaire, L.; Pitchon, V. Preparation and characterisation of activated Ni(Mn)/Mg/Al hydrotalcites for combustion catalysis. *Catal. Today* **2002**, *76*, 43–53.
8. Kovanda, F.; Jiratova, K.; Rymes, J.; Kolousek, D. Characterization of activated CuMgAl hydrotalcites and their catalytic activity in toluene combustion. *Appl. Clay Sci.* **2001**, *18*, 71–80.
9. Zhu, Z.; Lu, G.; Zhang, Z.; Guo, Y.; Guo, Y.; Wang, Y. Highly Active and Stable Co_3O_4/ZSM-5 Catalyst for Propane Oxidation: Effect of the preparation Method. *ACS Catal.* **2013**, *3*, 1154–1164.
10. Tang, C.-W.; Kuo, M.-C.; Lin, C.-J.; Wang, C.-B.; Chien, S.-H. Evaluation of carbon monoxide oxidation over CeO_2/Co_3O_4 catalysts: Effect of ceria loading. *Catal. Today* **2008**, *131*, 520–525.
11. Liotta, L.F.; Ousmane, M.; di Carlo, G.; Pantaleo, G.; Deganello, G.; Boreave, A.; Giroir-Fendler, A. Catalytic Removal of Toluene over Co_3O_4–CeO_2 Mixed Oxide Catalysts: Comparison with Pt/Al_2O_3. *Catal. Lett.* **2008**, *127*, 270–276.

12. Liotta, L.F.; Wu, H.; Pantaleo, G.; Venezia, A.M. Co_3O_4 nanocrystals and Co_3O_4–MO_x binary oxides for CO, CH_4 and VOC oxidation at low temperatures: A review. *Catal. Sci. Technol.* **2013**, *3*, 3085–3102.
13. Genty, E.; Cousin, R.; Capelle, S.; Gennequin, C.; Siffert, S. Catalytic Oxidation of Toluene and CO over Nanocatalysts Derived from Hydrotalcite-Like Compounds ($X_6^{2+}Al_2^{3+}$): Effect of the Bivalent Cation. *Eur. J. Inorg. Chem.* **2012**, *2012*, 2802–2811.
14. Gennequin, C.; Siffert, S.; Cousin, R.; Aboukaïs, A. Co–Mg–Al Hydrotalcite Precursors for Catalytic Total Oxidation of Volatile Organic Compounds. *Top. Catal.* **2009**, *52*, 482–491.
15. Debecker, D.P.; Gaigneaux, E.M.; Busca, G. Exploring, tuning, and exploiting the basicity of hydrotalcites for applications in heterogeneous catalysis. *Chemistry* **2009**, *15*, 3920–3935.
16. Chang, K.S.; Song, H.; Park, Y.-S.; Woo, J.-W. Analysis of N_2O decomposition over fixed bed mixed metal oxide catalysts made from hydrotalcite-type precursors. *Appl. Catal. A* **2004**, *273*, 223–231.
17. Palacio, L.A.; Velásquez, J.; Echavarría, A.; Faro, A.; Ribeiro, F.R.; Ribeiro, M.F. Total oxidation of toluene over calcined trimetallic hydrotalcites type catalysts. *J. Hazard. Mater.* **2010**, *177*, 407–413.
18. Tanasoi, S.; Mitran, G.; Tanchoux, N.; Cacciaguerra, T.; Fajula, F.; Săndulescu, I.; Tichit, D.; Marcu, I.-C. Transition metal-containing mixed oxides catalysts derived from LDH precursors for short-chain hydrocarbons oxidation. *Appl. Catal. A* **2011**, *395*, 78–86.
19. Gennequin, C.; Barakat, T.; Tidahy, H.L.; Cousin, R.; Lamonier, J.-F.; Aboukaïs, A.; Siffert, S. Use and observation of the hydrotalcite "memory effect" for VOC oxidation. *Catal. Today* **2010**, *157*, 191–197.
20. Genty, E.; Cousin, R.; Capelle, S.; Siffert, S. Influence of Gold on Hydrotalcite-like Compound Catalysts for Toluene and CO Total Oxidation. *Catalysts* **2013**, *3*, 966–977.
21. Carpentier, J.; Lamonier, J.F.; Siffert, S.; Zhilinskaya, E.A.; Aboukaïs, A. Characterisation of Mg/Al hydrotalcite with interlayer palladium complex for catalytic oxidation of toluene. *Appl. Catal. A* **2002**, *234*, 91–101.
22. Kovanda, F.; Rojka, T.; Dobešová, J.; Machovič, V.; Bezdička, P.; Obalová, L.; Jirátová, K.; Grygar, T. Mixed oxides obtained from Co and Mn containing layered double hydroxides: Preparation, characterization, and catalytic properties. *J. Solid State Chem.* **2006**, *179*, 812–823.
23. Kovanda, F.; Koloušek, D.; Cílová, Z.; Hulínský, V. Crystallization of synthetic hydrotalcite under hydrothermal conditions. *Appl. Clay Sci.* **2005**, *28*, 101–109.
24. Ran, R.; Weng, D.; Wu, X.; Fan, J.; Qing, L. Rapid synthesis of $La_{0.7}Sr_{0.3}MnO_{3+\lambda}$ catalysts by microwave irradiation process. *Catal. Today* **2007**, *126*, 394–399.
25. Kaddouri, A.; Ifrah, S. Microwave-assisted synthesis of $La_{1-x}B_xMnO_{3.15}$ (B = Sr, Ag; x = 0 or 0.2) via manganese oxides susceptors and their activity in methane combustion. *Catal. Commun.* **2006**, *7*, 109–113.
26. Zhou, X.; Chen, Q.; Tao, Y.; Weng, H. Influence of ultrasound impregnation on the performance of Co/Zr/SiO_2 catalyst during Fischer-Tropsch synthesis. *Chin. J. Catal.* **2011**, *32*, 1156–1165.
27. Climent, M.; Corma, A.; Iborra, S.; Epping, K.; Velty, A. Increasing the basicity and catalytic activity of hydrotalcites by different synthesis procedures. *J. Catal.* **2004**, *225*, 316–326.

28. Benito, P.; Labajos, F.M.; Rives, V. Microwaves and layered double hydroxides: A smooth understanding. *Pure Appl. Chem.* **2009**, *81*, 1459–1471.
29. Rivera, J.; Fetter, G.; Bosch, P. Microwave power effect on hydrotalcite synthesis. *Microporous Mesoporous Mater.* **2006**, *89*, 306–314.
30. Pérez, A.; Lamonier, J.-F.; Giraudon, J.-M.; Molina, R.; Moreno, S. Catalytic activity of Co–Mg mixed oxides in the VOC oxidation: Effects of ultrasonic assisted in the synthesis. *Catal. Today* **2011**, *176*, 286–291.
31. Neto, O.R.; Ribeiro, N.F.P.; Perez, C.A.C.; Schmal, M.; Souza, M.M.V.M. Incorporation of cerium ions by sonication in Ni–Mg–Al layered double hydroxides. *Appl. Clay Sci.* **2010**, *48*, 542–546.
32. Mokhtar, M.; Saleh, T.S.; Ahmed, N.S.; Al-Thabaiti, S.A.; Al-Shareef, R.A. An eco-friendly *N*-sulfonylation of amines using stable and reusable Zn-Al-hydrotalcite solid base catalyst under ultrasound irradiation. *Ultrason. Sonochem.* **2011**, *18*, 172–176.
33. Fetter, G.; Hernández, F.; Maubert, A. Microwave irradiation effect on hydrotalcite synthesis. *J. Porous Mater.* **1997**, *30*, 27–30.
34. Lars, S.; Andersson, T. Reaction Networks in the Catalytic Vapor-Phase Oxidation of Toluene and Xylenes. *J. Catal.* **1986**, *98*, 138–149.
35. Kannan, S.; Swamy, C.S. Catalytic decomposition of nitrous oxide over calcined cobalt aluminum hydrotalcites. *Catal. Today* **1999**, *53*, 725–737.
36. Gabrovska, M.; Edreva-Kardjieva, R.; Tenchev, K.; Tzvetkov, P.; Spojakina, A.; Petrov, L. Effect of Co-content on the structure and activity of Co–Al hydrotalcite-like materials as catalyst precursors for CO oxidation. *Appl. Catal. A Gen.* **2011**, *399*, 242–251.
37. Pérez-Ramírez, J.; Mul, G.; Kapteijn, F.; Moulijn, J.A. *In situ* investigation of the thermal decomposition of Co–Al hydrotalcite in different atmospheres. *J. Mater. Chem.* **2001**, *11*, 821–830.
38. Babay, S.; Bulou, A.; Mercier, A.M.; Toumi, M. The decomposition of the layered double hydroxides of Co and Al: Phase segregation of a new single phase spinel oxide. *Spectrochim. Acta Part A* **2015**, *141*, 80–87.
39. Alvarez, A.; Ivanova, S.; Centeno, M.A.; Odriozola, J.A. Sub-ambient CO oxidation over mesoporous Co_3O_4: Effect of morphology on its reduction behavior and catalytic performance. *Appl. Catal. A* **2012**, *431–432*, 9–17.
40. Xie, X.; Li, Y.; Liu, Z.-Q.; Haruta, M.; Shen, W. Low-temperature oxidation of CO catalysed by Co_3O_4 nanorods. *Nature* **2009**, *458*, 746–749.
41. Arnoldy, P.; Moulijn, J.A. Temperature-Programmed Reduction of CoO/Al_2O_3 Catalysts. *J. Catal.* **1985**, *93*, 38–54.
42. Sexton, B.A.; Hughes, A.E.; Turney, T.W. An XPS and TPR Study of the Reduction of Promoted Cobalt-Kieselguhr Fisher-Tropsch Catalysts. *J. Catal.* **1986**, *406*, 390–406.
43. Busca, G.; Finocchio, E.; Ramis, G.; Ricchiardi, G. On the role of acidity in catalytic oxidation. *Catal. Today* **1996**, *32*, 133–143.
44. Cook, K.M.; Poudyal, S.; Miller, J.T.; Bartholomew, C.H.; Hecker, W.C. Reducibility of alumina-supported cobalt Fischer-Tropsch catalysts: Effects of noble metal type, distribution, retention, chemical state, bonding, and influence on cobalt crystallite size. *Appl. Catal. A* **2012**, *449*, 69–80.

45. Dupin, J.-C.; Gonbeau, D.; Vinatier, P.; Levasseur, A. Systematic XPS studies of metal oxides, hydroxides and peroxides. *Phys. Chem. Chem. Phys.* **2000**, *2*, 1319–1324.
46. Delimaris, D.; Ioannides, T. VOC oxidation over MnO_x–CeO_2 catalysts prepared by a combustion method. *Appl. Catal. B Environ.* **2008**, *84*, 303–312.
47. Liu, Y.; Dai, H.; Deng, J.; Xie, S.; Yang, H.; Tan, W.; Han, W.; Jiang, Y.; Guo, G. Mesoporous Co_3O_4-supported gold nanocatalysts: Highly active for the oxidation of carbon monoxide, benzene, toluene, and *O*-xylene. *J. Catal.* **2014**, *309*, 408–418.
48. Sampanthar, J.T.; Zeng, H.C. Synthesis of $Co^{II}Co^{III}_{2-x}Al_xO_4$-$Al_2O_3$ Nanocomposites via Decomposition of $Co^{II}_{0.73}Co^{III}_{0.27}(OH)_{2.00}(NO_3)_{0.23}(CO_3)_{0.02}\cdot 0.5H_2O$ in a Sol-Gel-Derived γ-Al_2O_3 Matrix. *Chem. Mater.* **2001**, *13*, 4722–4730.
49. Garcia, T.; Agouram, S.; Sánchez-Royo, J.F.; Murillo, R.; Mastral, A.M.; Aranda, A.; Vázquez, I.; Dejoz, A.; Solsona, B. Deep oxidation of volatile organic compounds using ordered cobalt oxides prepared by a nanocasting route. *Appl. Catal. A* **2010**, *386*, 16–27.
50. Cheng, J.; Yu, J.; Wang, X.; Li, L.; Li, J.; Hao, Z. Novel CH_4 Combustion Catalysts Derived from Cu-Co/*X*-Al (*X* = Fe, Mn, La, Ce) Hydrotalcite-like Compounds. *Energy Fuels* **2008**, *22*, 65–67.
51. Solsona, B.; Davies, T.E.; Garcia, T.; Vázquez, I.; Dejoz, A.; Taylor, S.H. Total oxidation of propane using nanocrystalline cobalt oxide and supported cobalt oxide catalysts. *Appl. Catal. B* **2008**, *84*, 176–184.
52. Bahlawane, N. Kinetics of methane combustion over CVD-made cobalt oxide catalysts. *Appl. Catal. B* **2006**, *67*, 168–176.